Effect of Ultrasound on the Electrochemical Performance and Corrosion Resistance of the Ti/Sn−Ru−CoOₓ Electrode

Chen Yang, Ruidong Xu, Buming Chen,* Sheng Chen, and Zhongcheng Guo

Read Online

ACCESS | Metrics & More | Article Recommendations

ABSTRACT: A ternary mixed metal oxide coating of Sn−Ru−CoOₓ was prepared by ultrasonic treatment. The effect of ultrasound on the electrochemical performance and corrosion resistance of the electrode was investigated in this paper. Results showed that the electrode prepared by ultrasonic pretreatment demonstrated more uniform oxide dispersion on the surface of the coating, smaller grain growth, and more compact surface morphology compared with the anode prepared without ultrasonic pretreatment. At the same time, the best electrocatalytic performance was obtained by the ultrasonically treated coating. The chlorine evolution potential was reduced by 15 mV. The anode prepared by ultrasonic pretreatment had a service life of 160 h, which was 46 h longer than the anode prepared without ultrasonic pretreatment.
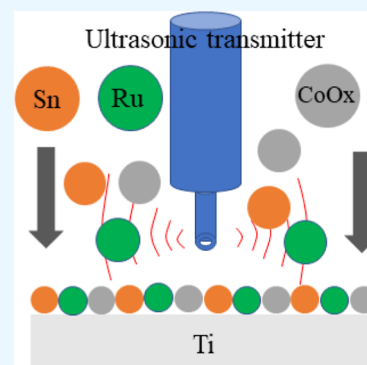
1. INTRODUCTION

In the electrolytic manganese production industry, the choice of anode materials is critical. Graphite electrodes are used in the conventional electrolytic manganese industry,[1] but lead-based alloy electrode[2] and titanium-based coated electrodes[3] are emerging and gaining popularity. However, the graphite anode has high energy consumption. The simple graphite electrode has a short service life in electrolytic manganese and dissolves into the solution, causing contamination of the cathode product and the electrolyte.[4] Lead-based alloy anodes may have a powdery shape in solution during electrolysis. It has high electrochemical activity of MnO_2 formation, and MnO_2 particles contain lead impurities, which can lead to the consumption of a large amount of electric energy and complicated lead removal.[2] However, the titanium-based coating anode is dimensionally stable. It ensures that the electrolysis operation is carried out under stable tank voltage, low power consumption, and long life.[5] It can overcome the dissolution of graphite electrodes and lead-based alloy electrodes and avoid contamination of the electrolyte, thereby improving product quality. It can increase current density and increase production efficiency.

Oxide coatings on titanium substrates are also used in the chlor-alkali industry as anodes for electrochemical processes.[6] The oxide coating (RuO_2,[7] MnO_2,[8] TiO_2,[9] and SnO_2[10]) consists of a highly corrosion resistant material. The RuO_2-based anode has extremely high stability against chlorine evolution, but its cost is high and its chlorine evolution overpotential is low.[11,12] The SnO_2-based anode is inexpensive and non-toxic, and it is considered the most promising anode

that has been studied in depth.[13] However, the most deadly disadvantage of SnO_2-based anodes is their short life.[14] Therefore, the two oxides of SnO_2 and RuO_2 are mixed together. They both have a rutile structure, and a solid solution can be obtained.[15−21] The electrode simultaneously possesses the properties of a single oxide, which is more advantageous for the electrochemical reaction in chlorine evolution. The Co-based titanium-based ruthenium metal coating is also used in the chloride system. The titanium-based Co−Zn−Zr oxide chlorination electrode studied by Harrison et al.[22] is comparable with the titanium ruthenium anode.

The morphology and microstructure uniformity of the oxide coating have an important influence on the service life and electrochemical performance of the electrode. In this work, the electrocatalytic activity of the mixed oxide was systematically studied to clarify the effect of ultrasonic treatment and non-precursor on the mixed oxide electrode. The effect of ultrasonic treatment on the electrocatalytic activity and stability of $SnO_2−RuO_2−CoO_x$ oxide coatings in the HCl−NH_4Cl medium was also investigated. The prepared mixed oxide coating was subjected to cyclic voltammetry (CV) to examine its electrochemically active surface area.[23,24] The change in electrocatalytic activity due to compositional
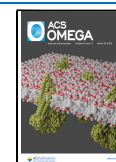
changes (i.e., the release rate of Cl_2) was investigated by the anodic polarization measurement. The life of the anode and the stability of the coating were evaluated by an accelerated life test.

2. RESULTS AND DISCUSSION

2.1. XRD Analysis of the Sn−Ru−CoO$_x$ Layer.
Figure 1 shows that the crystal form of the sonicated and non-sonicated
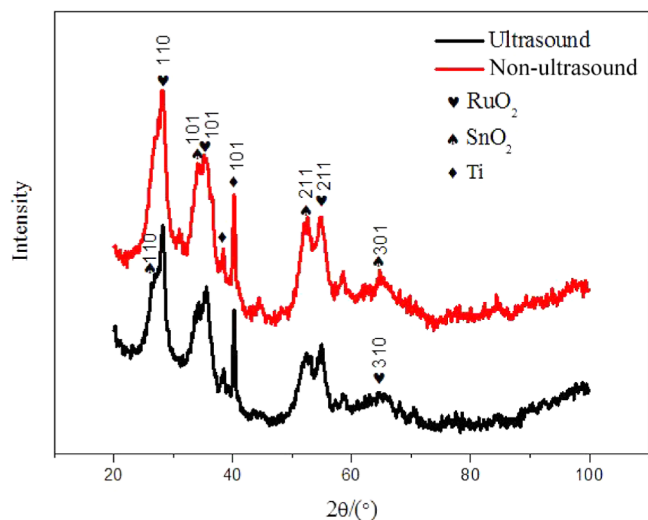

Figure 1. XRD patterns of Ti/Sn−Ru−CoO$_x$ electrodes prepared under ultrasound and non-ultrasound.

coating surface did not change. The three main diffraction peaks of the ultrasonic and non-ultrasonic crystals had crystal spacings d of (3.247, 3.242 Å), (2.576, 2.566 Å), and (1.714, 1.713 Å), with a distance d between RuO_2 (3.182, 2.557, and 1.691 Å, respectively) of the rutile structure and SnO_2 (3.347, 2.663, and 1.764 Å, respectively). It was mainly close to the intercrystalline distance d of RuO_2. At the same time, the ionic radii of Sn^{4+} and Ru^{4+} were very close to 0.071 and 0.065 nm, respectively. Given that both SnO_2 and RuO_2 have a rutile structure, a solid solution could easily form. As shown in Figure 1, the solid solution was a rutile solid solution, so the solid solution structure was mainly a ruthenium-based solid solution. By comparing the crystal spacing between the two, the crystal surface density of the electrode prepared by ultrasound was greater, which indicated that the electrode coating prepared by ultrasonic treatment grew more densely on the (110), (101), and (211) crystal planes in a solid solution. The diffraction peak of Co did not appear in the X-ray diffraction (XRD) pattern. It may be because the content of cobalt was too small, and the oxides of tin, ruthenium, and cobalt were mixed crystals, which inhibited the growth of cobalt oxides and were amorphous in the coating. Moreover, its oxide diffraction peak did not appear in the spectrum. The diffraction peak of the Ti metal appeared in the XRD pattern. At the same time, the intensity of each diffraction peak of ultrasonic treatment was much weaker than the peak of non-sonication, especially for Ti metal. Diffraction peaks indicated that the ultrasonically treated coating exhibited better dispersion properties[27] and provided better protection than the non-sonicated coating.[28−30]

2.2. Surface Morphology of Interlayer.
As an active layer of the electrodeposited manganese industry, a coarse 3D

dense structure is preferred to increase the electrocatalytic activity and service life of the active layer. The addition of Co completely changes the surface morphology of the coating. Microscopic morphology revealed that Co addition converted the coating into a 3D spherical shape. Given the addition of Co, the coating demonstrated a spherical packing arrangement, so it was effectively released, and there is no deeper crack of the turtle than Sn−RuO_2 without Co addition. It could better protect the substrate from corrosion by solution and provide an active surface. A comparison of Figure 2a,c showed that the
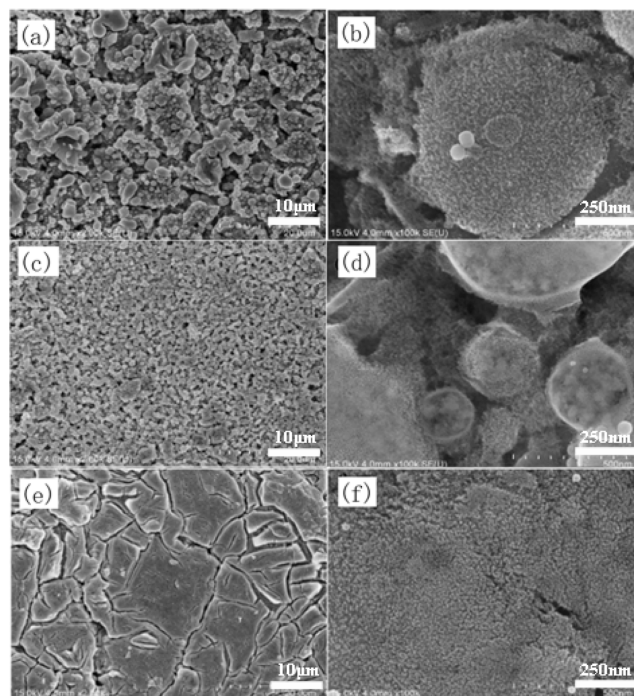

Figure 2. SEM images of non-ultrasound- and ultrasound-treated Sn−Ru−CoO$_x$ coatings and evolution of the crystal grain size: (a,b) non-ultrasound, (c,d) ultrasound, and (e,f) Sn−RuO_2.

latter had a denser surface than the former. As shown in Figure 2b,d, the coating prepared by ultrasonic pretreatment had finer grains than that without ultrasonic treatment. Thus, the coating prepared by ultrasonic pretreatment had a better morphology than that without ultrasonic treatment (Figure 2).

2.3. Chlorine Evolution Activity of the Ti/Sn−Ru−CoO$_x$ Electrode.
Figure 3 shows the anodic polarization curves for both ultrasonic and non-ultrasonic pretreatment. Under the electrodeposited manganese current density of 500 A m^{-2}, the chlorine gas deposition potential on the electrode prepared by ultrasonic pretreatment was lower than that prepared without ultrasonic pretreatment. Given that the metal particles on the surface of the electrode prepared by ultrasonic pretreatment were more uniformly distributed and the crystal grains were finer, more active sites could be provided for the chlorine gas release reaction, thereby increasing the electrocatalytic activity. The chlorine precipitation potential of the electrode prepared by ultrasonic pretreatment was 15 mV lower than that of the electrode prepared without ultrasonic pretreatment, indicating that ultrasonic pretreatment could effectively improve the surface shape and appearance of the Ti/Sn−Ru−CoO$_x$ electrode, thereby increasing the electrocatalytic activity.
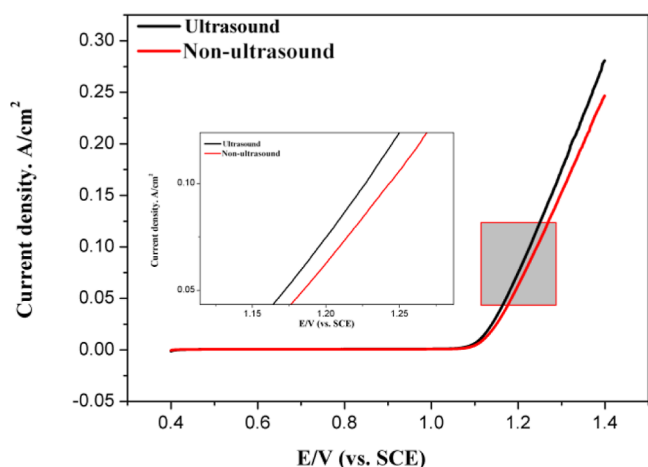
Figure 3. Anodic polarization curves of different Ti/Sn−Ru−CoO$_x$ samples under a scan rate of 5 mV s^{-1}.
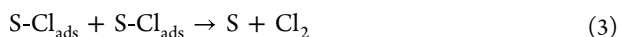
The anodic polarization curve was converted into the Tafel curve (η−lg i) and linearly fitted using Origin software to obtain a and b values, and the results are displayed in Figure 3 and Table 1. Table 1 shows that the electrode prepared by

Table 1. Overpotential and Kinetic Parameters for Chlorine Evolution on Various Ti/Sn−Ru−CoO$_x$ Samples

| anode sample | H (V) | | a/V | b/V dec^{-1} |
	500 A/m^2	1000 A/m^2		
ultrasound	0.163	0.246	0.520	0.274
non-ultrasound	0.187	0.265	0.524	0.259

ultrasonic pretreatment exhibited the lowest CER values (0.163 and 0.246 V) under 500 and 1000 A m^{-2}, indicating the high probability of the chlorine evolution reaction. Table 1 shows that a of the ultrasound electrode and non-ultrasound electrode differed by 0.004.

The mechanism of chlorine evolution on the Ti/Sn−Ru−CoO$_x$ electrode in an acid solution may be as follows[1−32]

$$S + Cl^- \rightarrow S\text{-}Cl_{ads} + e \tag{1}$$

$$S\text{-}Cl_{ads} + Cl^- \rightarrow S + Cl_2 \tag{2}$$

$$S\text{-}Cl_{ads} + S\text{-}Cl_{ads} \rightarrow S + Cl_2 \tag{3}$$

The larger the S value of the Ti/Sn−Ru−CoO$_x$ electrode, the more favorable the precipitation of chlorine and the greater the number of high electrochemical active sites on the surface of the electrode (Figure 4).

The surface roughness of AC impedance is used to estimate the specific surface area of the electrode.

$$Q_{dl} = (C_{dl})^n [(R_S)^{-1} + (R_t)^{-1}]^{(1-n)} \tag{4}$$

Therefore, according to the model described in formula 4, the double layer capacitance C_{dl} value can be obtained by calculating the Q_{dl} value. The Q_{dl} value is obtained by nonlinear least squares (CNLS) fitting. Alves proposed a new method to characterize the roughness/porosity of oxide electrodes. According to the proposed method, C_{dl} can be used as a relative method to characterize electrode surface roughness. The anode roughness (RF) can be calculated by formula 5.
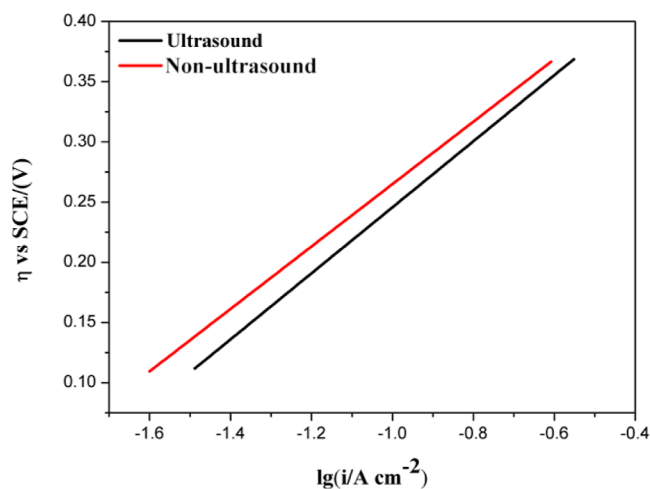

Figure 4. Tafel curves of various Ti/Sn−Ru−CoO$_x$ samples.

$$RF = \frac{C_{dl}}{C^*} \tag{5}$$

In the formula, C^* represents a capacitance reference ratio. For a smooth mercury electrode, C^* is 20 μF cm^{-2}. Roughness values obtained from anodic oxide films are often used to characterize the micro morphology of electrodes.[33]

The voltammetric charge (q^*) was calculated by eq 6

$$(q^*)^{-1} = (q_\tau)^{-1} + \kappa v^{1/2} \tag{6}$$

The voltammetric curves of 100 mV/s Ti/Sn−Ru−CoO$_x$ samples over the entire potential range of 0.4−1.1 V under different sweep speeds are exhibited in Figure 5. Here, q^* is
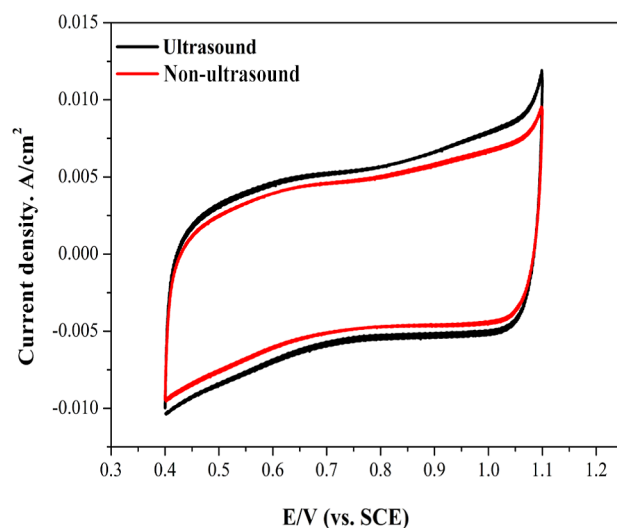

Figure 5. CV of Ti/Sn−Ru−CoO$_x$ coatings prepared under ultrasound and non-ultrasound.

measured in an acid NH$_4$Cl solution to determine the electrochemically active surface area of the Ti/Sn−Ru−CoO$_x$ electrode. Therefore, the capacitance region q^* of Ti/Sn−Ru−CoO$_x$ can be defined as the electrochemically active surface area of Ti/Sn−Ru−CoO$_x$ in the chlorate electrolyte. Through the measurement of the active area, the effective surface area of the ultrasound electrode was found to be higher than that of the non-ultrasound electrode. Therefore, the electrode with a
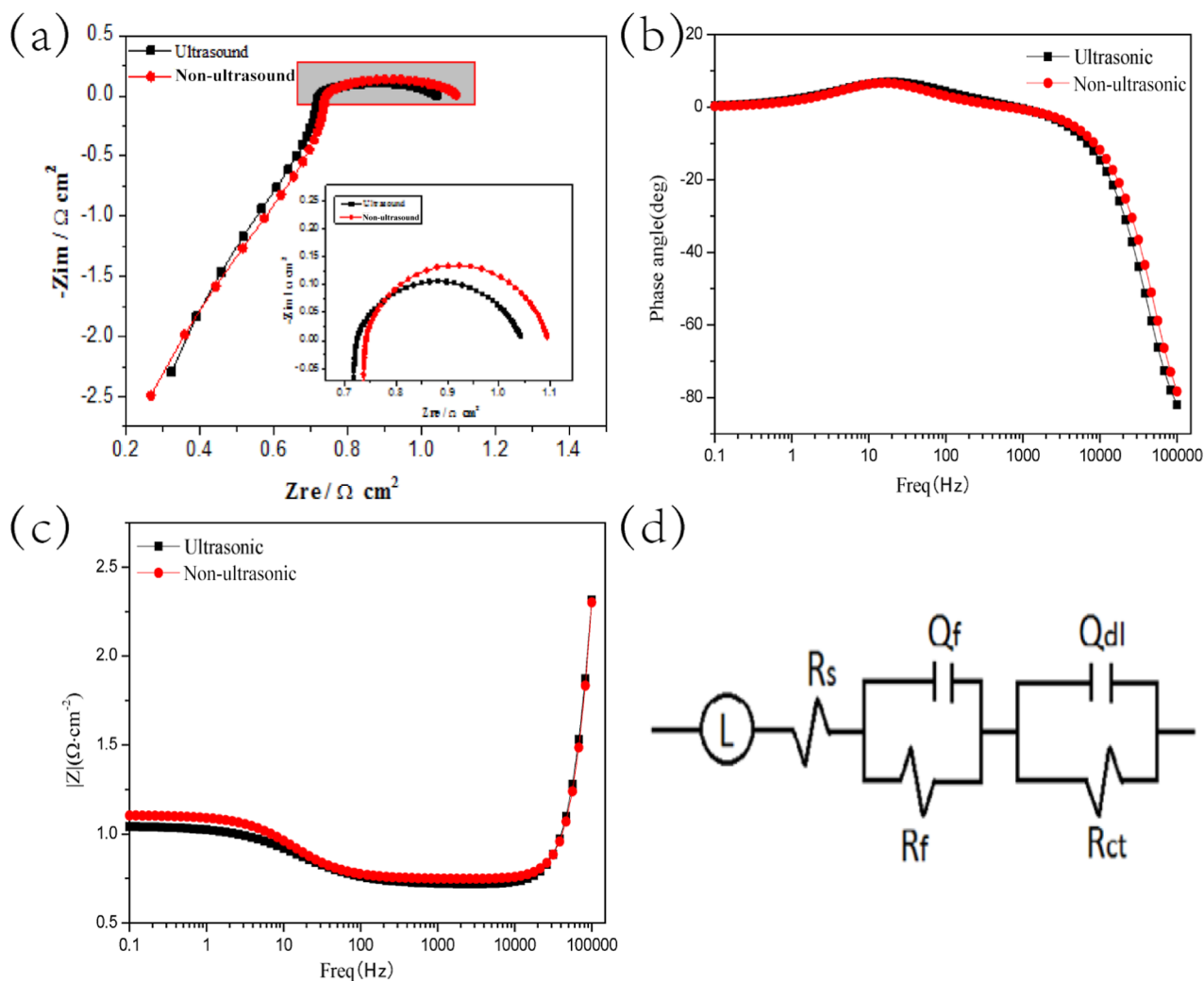
Figure 6. Nyquist diagrams (a) and Bode diagrams (b,c) for the Ti/Sn−Ru−CoO$_x$ anodes, and AC impedance fitting circuit diagram (d).

Table 2. Fitting Parameter of EIS Curves

anode sample	L (μH)	R_s (Ω cm^2)	Q_f (Ω^{-1} cm^{-2} S^n)	n_1	R_f (Ω cm^2)	Q_{dl} (Ω^{-1} cm^{-2} S^n)	n_2	R_{ct} (Ω cm^2)
ultrasound	4.226	0.01	2.454×10^{-6}	0.729	0.3296	0.1115	1	0.7162
non-ultrasound	4.741	0.01	1.57×10^{-6}	0.821	0.3591	0.0754	1	0.9806

low chlorine evolution potential was confirmed to have more active sites and higher chlorine evolution activity.

2.4. Electrochemical Impedance Spectroscopy. The Bode plot and Nyquist plot are shown in Figure 6. The low-frequency arc reflects the evolution of chlorine gas, whereas the high-frequency arc is related to the performance of the oxide film. In addition, the anodes with different surface treatments have similar profiles and values; they have the same surface condition and equivalent circuit model, which can be described as $LR_s(R_{ct}Q_{dl})$ (R_fQ_f). R_s, R_{ct}, and R_f represent the resistance of the solution, the charge transfer resistance, and the oxide film resistance for oxygen evolution, respectively. In general, Q_{dl} and Q_f are used instead of double-layer capacitors and thin-film capacitors to produce the best results. Porosity and surface non-uniformity of oxide electrodes lead to good fitting results. The inductance of L may be the result of the porous nature of oxide electrodes and test systems. Q_{dl} and R_{ct} shown in Table 2 can be used to express the ability of an electrochemical reaction and the resistance of an obstacle. An anode with a

sonicated substrate had the highest Q_{dl} and the lowest R_{ct} value among all anodes, which demonstrated that it was the strongest support for electrochemical reactions among all anodes. The trend of these two parameters was closely consistent with the q^* value of the CV integral. Figure 6b,c are Bode diagrams, showing the relationship between frequency and constant phase angle, frequency and resistance, respectively. It can be seen from Figure 6b that the double line segment results show that the system corresponds to two time constants, that is, two constant phase components. As can be seen in Figure 6c, the mass transfer resistance R_{ct} of low-frequency ultrasound is lower than that of non-ultrasound. This can be seen in ref 24.

2.5. Corrosion Resistance Evaluation. Service life is one of the important factors in evaluating corrosion resistance in practical applications of electrodes. As shown in Figure 6, the electrode prepared by sonication had the longest life of 160 h and exhibited good stability, which was 46 h longer than the electrode life (114 h) of the electrode prepared without

sonication. The results showed that the electrode prepared by ultrasonic treatment could improve the electrochemical stability of the Ti/Sn−Ru−CoO$_x$ film. A possible reason for prolonging the service life is that the ultrasonic treatment improved its morphological structure; scanning electron microscopy (SEM) confirmed this conclusion. The corrosion life of the ultrasonically prepared electrode was longer than that of the non-ultrasonically prepared electrode. This result could be attributed to the fact that the oxide coating grains of the ultrasonic preparation electrode were fine, which reduced the gap between the grain boundaries and made the electrode surface dense (Figure 7).
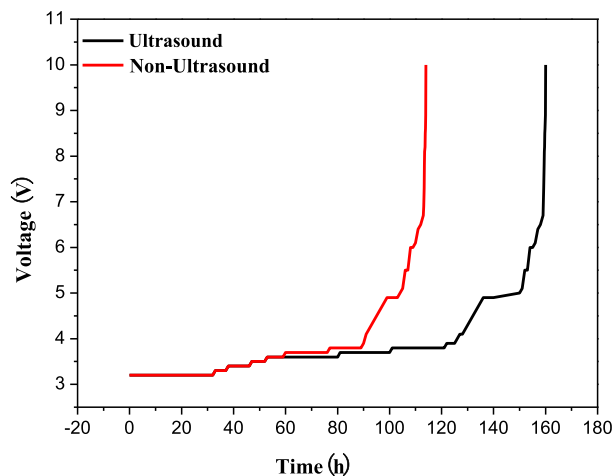

Figure 7. Accelerated life test of Ti/Sn−Ru−CoO$_x$ coatings prepared under ultrasound and non-ultrasound.

3. CONCLUSIONS

In summary, we investigated the role of the ultrasonic pretreatment to prepare the Ti/Sn−Ru−CoO$_x$ electrode in manganese electrowinning. XRD results showed no change in the phase of the ultrasonically pretreated electrode and the non-sonically pretreated electrode, but the ultrasonically pretreated electrode oxide coating was more evenly dispersed than its counterpart. The kinetics of chlorine evolution, microscopic surface morphology, and corrosion results of the anode layer indicated that the electrode prepared by ultrasonic pretreatment was better than that prepared by non-sonication pretreatment. Furthermore, the accelerated life of the electrode subjected to ultrasonic pretreatment was 160 h, exhibiting good stability. This value was 46 h more than that prepared without ultrasonic pretreatment.

4. EXPERIMENTAL SECTION

First, the titanium base was pretreated as described in Li's research.[25] Pretreatment comprised four steps: alkali leaching to remove oil, mixed acid (VHF/VHNO$_3$/VH$_2$O = 1:4:5) etching to remove oxides, HCl etching to form a rough surface, and storing in ethanol solution and 2% oxalic acid. Second, the precursor solutions of SnCl$_4$·5H$_2$O, RuCl$_3$·3H$_2$O, and CoCl$_2$·6H$_2$O prepared by Sn−Ru−CoO$_x$ were dissolved in the mixed solvent at a molar ratio of 6:1:1. One was completely and uniformly dissolved under ultrasound, and the other was completely and uniformly dissolved under non-ultrasound treatment to obtain a coating solution, which was evenly brushed on the acid-etched titanium plate. The plates were

then placed in an oven at 100 °C, removed after 5 min, and left at room temperature. The coating was subjected to high-temperature calcination at 400 °C for 10 min. The brushing, drying, and calcination steps were repeated 13 times. Finally, the coating was placed in a muffle furnace for 1 h.

SEM was used to characterize the microstructure of the Sn−Ru−CoO$_x$ electrode. XRD was used for phase composition analysis. The electrochemical performance was determined on an electrochemical workstation (CHI760E, Chenhua, China) using a three-electrode system. The electrolyte solution was composed of 1.5 M HCl and 1 M NH$_4$Cl, and the temperature was normal temperature.[26] The prepared electrode was used as the anode. In this work, 1.5 M HCl and 1 M NH$_4$Cl were used as the electrolyte. The current density was maintained at 1 A cm^{-2}. The cell voltage (U) versus service time (t) was simultaneously recorded.

■ **AUTHOR INFORMATION**

Corresponding Author

   Buming Chen − *Faculty of Metallurgical and Energy Engineering, Kunming University of Science and Technology, Kunming 650093, China; Kunming Hengda Technology Co. Ltd., Kunming 650106, China;* ◉ orcid.org/0000-0002-3444-0835; Email: bumchen@kust.edu.cn

Authors

   Chen Yang − *Faculty of Metallurgical and Energy Engineering, Kunming University of Science and Technology, Kunming 650093, China; Yunnan Jinding Zinc Co., Ltd., Lanping, Yunnan 671400, China*
   Ruidong Xu − *Faculty of Metallurgical and Energy Engineering, Kunming University of Science and Technology, Kunming 650093, China*
   Sheng Chen − *Faculty of Metallurgical and Energy Engineering, Kunming University of Science and Technology, Kunming 650093, China*
   Zhongcheng Guo − *Faculty of Metallurgical and Energy Engineering, Kunming University of Science and Technology, Kunming 650093, China; Kunming Hengda Technology Co. Ltd., Kunming 650106, China*

Complete contact information is available at:
https://pubs.acs.org/10.1021/acsomega.3c00047

Author Contributions

C.Y.: conceptualization, methodology, and writing—original draft. R.X.: conceptualization, methodology, software, and analysis. B.C.: writing—review and editing, conceptualization, methodology, formal analysis, investigation, and supervision. S.C.: writing—review and editing, conceptualization, methodology, and experiments. Z.G.: writing—review and editing, conceptualization, methodology, formal analysis, investigation, and supervision.

Notes

The authors declare no competing financial interest.

■ REFERENCES

(1) Lewis, J. E.; Scaife, P. H.; Swinkels, D. A. J. Electrolytic manganese metal from chloride electrolytes. I. Study of deposition conditions. *J. Appl. Electrochem.* **1976**, *6*, 199−209.

(2) Zhang, W.; Cheng, C. Y. Manganese metallurgy review. Part I: Leaching of ores/secondary materials and recovery of electrolytic/ chemical manganese dioxide. *Hydrometallurgy* **2007**, *89*, 137−159.

(3) Wei, Q.; Ren, X.; Du, J.; Wei, S.; Hu, S. Study of the electrodeposition conditions of metallic manganese in an electrolytic membrane reactor. *Miner. Eng.* **2010**, *23*, 578−586.

(4) Kim, H. S.; Kim, H. J.; Cho, W. I.; Cho, B. W.; Ju, J. B. Discharge characteristics of chemically prepared MnO2 and electrolytic MnO2 in non-aqueous electrolytes. *J. Power Sources* **2002**, *112*, 660−664.

(5) Subba Rao, A. N.; Venkatarangaiah, V. T. Metal oxide-coated anodes in wastewater treatment. *Environ. Sci. Pollut. Res.* **2014**, *21*, 3197−3217.

(6) Trasatti, S. Electrocatalysis: Understanding the success of DSA. *Electrochim. Acta* **2000**, *45*, 2377−2385.

(7) Ribeiro, J.; De Andrade, A. R. Characterization of RuO[sub 2]- Ta[sub 2]O[sub 5] Coated Titanium Electrode. *J. Electrochem. Soc.* **2004**, *151*, D106−D112.

(8) Zhou, X. L.; Ye, Z. G.; Hua, X. Z.; Zou, A. H.; Dong, Y. H. Electrocatalytic activity and stability of Ti/IrO2 + MnO2 anode in 0.5 M NaCl solution. *J. Solid State Electrochem.* **2010**, *14*, 1213−1219.

(9) Hoseinieh, S. M.; Ashrafizadeh, Z. F.; Maddahi, M. H. A. A Comparative Investigation of the Corrosion Behavior of RuO[sub 2]- IrO[sub 2]-TiO[sub 2] Coated Titanium Anodes in Chloride Solutions. *J. Electrochem. Soc.* **2010**, *157*, No. E50.

(10) Battaglin, G.; Rosestolato, D.; Ferro, S.; De Battisti, A. Characterization of IrO2-SnO2 Films Prepared by Physical Vapor Deposition at Ambient Temperature. *Electrocatalysis* **2013**, *4*, 358− 366.

(11) Moradi, F.; Dehghanian, C. Addition of IrO2 to RuO2+TiO2 coated anodes and its effect on electrochemical performance of anodes in acid media. *Prog. Nat. Sci.: Mater. Int.* **2014**, *24*, 134−141.

(12) Kim, K. W.; Lee, E. H.; Kim, J. S.; Shin, K. H.; Jung, B. I. A study on performance improvement of Ir oxide-coated titanium electrode for organic destruction. *Electrochim. Acta* **2002**, *47*, 2525− 2531.

(13) Christensen, P. A.; Zakaria, K.; Christensen, H.; Yonar, T. The Effect of Ni and Sb Oxide Precursors, and of Ni Composition, Synthesis Conditions and Operating Parameters on the Activity, Selectivity and Durability of Sb-Doped SnO2Anodes Modified with Ni. *J. Electrochem. Soc.* **2013**, *160*, H405−H413.

(14) Chen, A.; Zhu, X.; Xi, J.; Qin, H.; Ji, Z.; Zhu, K. Effects of nickel doping on the preferred orientation and oxidation potential of Ti/Sb SnO2 anodes prepared by spray pyrolysis. *J. Alloys Compd.* **2016**, *684*, 137−142.

(15) Kolesnikov, V. A.; Novikov, V. T.; Isaev, M. K.; Alekseeva, T. V.; Kolesnikov, A. V. Investigation of electrodes with an active layer of a mixture of the oxides TiO₂, RuO₂, SnO₂. *Glass. Ceram* **2018**, *75*, 148.

(16) Petrykin, V.; Kateina, M.; Okube, M.; Mukerjee, S.; Krtil, P. Local structure of Co doped RuO₂ nanocrystalline electrocatalytic materials for chlorine and oxygen evolution. *Catal. Today* **2013**, *202*, 63.

(17) Mondelli, C.; Amrute, A. P.; Krumeich, F.; Schmidt, T.; Pérez- Ramírez, J. Cover Picture: Shaped RuO2/SnO2-Al2O3 Catalyst for Large-Scale Stable Cl2 Production by HCl Oxidation (ChemCatChem 4/2011). *Chemcatchem* **2011**, *3*, 617.

(18) Chen, S.; Zheng, Y.; Wang, S.; Chen, X. Ti/RuO2-Sb2O5- SnO2 electrodes for chlorine evolution from seawater. *Chem. Eng. J.* **2011**, *172*, 47−51.

(19) Vázquez-Gómez, L.; Horváth, E.; Kristóf, J.; Rédey, A.; De Battisti, A. D. Investigation of IrO2-SnO2 thin film evolution from aqueous media. *Appl. Surf. Sci.* **2006**, *253*, 1178−1184.

(20) Gaudet, J.; Tavares, A. C.; Trasatti, S.; Guay, D. Physicochemical Characterization of Mixed RuO2−SnO2 Solid Solutions. *Chem. Mater.* **2005**, *17*, 1570−1579.

(21) Nanni, L.; Polizzi, A. D.; Benedetti, S.; De Battisti, A. Morphology, Microstructure, and Electrocatalytic Properties of RuO2 - SnO2 Thin Films. *J. Electrochem. Soc.* **1999**, *146*, 220−225.

(22) Harrison, J. A.; Caldwell, D. L.; White, R. E. Electrocatalysis and the chlorine evolution reaction. *Electrochim. Acta* **1983**, *28*, 1561−1568.

(23) Chen, Y.; Hong, L.; Xue, H.; Han, W.; Wang, X.; Sun, J.; Li, J. Preparation and characterization of TiO2-NTs/SnO2-Sb electrodes by electrodeposition. *J. Electroanal. Chem.* **2010**, *648*, 119−127.

(24) Chen, B.; Wang, S.; Liu, J.; Huang, H.; Dong, C.; He, Y.; Yan, W.; Guo, Z.; Xu, R.; Yang, H. Corrosion resistance mechanism of a novel porous Ti/Sn-Sb-RuOx/β-PbO2 anode for zinc electrowinning. *Corros. Sci.* **2018**, *144*, 136−144.

(25) Li, L.; Huang, Z.; Fan, X.; Zhang, Z.; Dou, R.; Wen, S.; Chen, Y.; Chen, Y.; Hu, Y. Preparation and Characterization of a Pd modified Ti/SnO 2 -Sb anode and its electrochemical degradation of Ni-EDTA. *Electrochim. Acta* **2017**, *231*, 354−362.

(26) Xu, R.; Huang, L.; Zhou, J.; Zhan, P.; Guan, Y.; Kong, Y. Effects of tungsten carbide on electrochemical properties and microstructural features of Al/Pb-PANI-WC composite inert anodes used in zinc electrowinning. *Hydrometallurgy* **2012**, *125-126*, 8−15.

(27) Yu, J.; Hai, Y.; Cheng, B. Enhanced Photocatalytic H2- Production Activity of TiO2 by Ni(OH)2 Cluster Modification. *J. Phys. Chem. C* **2011**, *115*, 4953−4958.

(28) Xu, J.; Ding, D.; Yin, G.; Tian, Z.; Zhang, S.; Hong, Z.; Huang, F. Capacitive lithium storage of lithiated mesoporous titania. *Mater. Today Energy* **2018**, *9*, 240−246.

(29) Xu, J.; Huang, J.; Zhang, S.; Hong, Z.; Huang, F. Understanding the surface reduction of nano rutile and anatase: selective breaking of Ti-o bonds. *Mater. Res. Bull.* **2019**, *121*, 110617.

(30) Xu, J.; Tian, Z.; Yin, G.; Lin, T.; Huang, F. Controllable reduced black titania with enhanced photoelectrochemical water splitting performance. *Dalton Trans.* **2017**, *46*, 1047.

(31) Ghany, N.; Meguro, S.; Kumagai, N.; Asami, K.; Hashimoto, K. Anodically deposited Mn-Mo-Fe oxide anodes for oxygen evolution in hot seawater electrolysis. *Mater. Trans.* **2003**, *44*, 2114−2123.

(32) Xie, X.; Chang, L.; Chen, B.; Li, J.; Huang, H.; Guo, Z.; He, Y. Effects of coating precursor states on performance of titanium-based metal oxide coating anode for Mn electrowinning. *Electrochim. Acta* **2021**, *400*, 139459.

(33) Alves, V. A.; Silva, L. A.; Boodts, J. Surface characterization of IrO₂/TiO₂/CeO₂ oxide electrodes. *Electrochim. Acta* **1998**, *44*, 1525− 1534.